# Hydraulic redistribution in mangroves: time-lapse electrical resistivity reveals diel patterns of subsurface salt mobilization consistent with exchange of water between trees and sediments

Christine Downs[1,1], Ken Krauss[2], and Sarah Kruse[3,3]

[1]Sandia National Laboratories
[2]U.S Geological Survey
[3]University of South Florida,Massachusetts Institute of Technology

November 30, 2022

## Abstract

A 24-hour 2D time-lapse electrical resistivity imaging (ERI) survey was conducted in an altered mangrove forest on a barrier island in southeast Florida, USA, to (1) assess the method's utility in hypersaline conditions and (2) understand how trees respond to hypersaline conditions. ERI measurements serve as a proxy for pore water salinity and saturation. Here, resistivity changes suggest a lag between the tidal cycle and changes in ground resistivity. ERI data show that overall changes within 24 hours are very small, but there is more variability in resistivity in the root zone of mangroves than in open salt flat portions along a fixed transect. Two to three hours after sunset, root zone resistivity increased from initial, midday conditions. Overnight, the root zone was less resistive than midday. By sunrise, root zone resistivity was once again higher than initial conditions. Measurements from the salt flat where roots are absent remained generally constant throughout the survey. Thus, changes in resistivity over time are inferred to reflect mangrove tree physiological influences related to diel water use. A mechanistic explanation for the decreased resistivity two hours after sunset from the re-distribution of salts to the soil around the roots is the Cohesion-Tension Theory, which suggests that trees continue water uptake after sunset to balance the pressure after leaf stomates have closed. The corresponding overnight drop in ground resistivity just prior to sunrise may be explained by redistribution of freshwater from the tree to the soil that was delayed until the early morning hours. The limited period of data acquisition limits definitive data interpretations, but the study illustrates the monitoring potential of ERI in hypersaline environments such as a mangrove forest.

## Hosted file

`essoar.10511305.2.docx` available at https://authorea.com/users/560132/articles/608325-hydraulic-redistribution-in-mangroves-time-lapse-electrical-resistivity-reveals-diel-patterns-of-subsurface-salt-mobilization-consistent-with-exchange-of-water-between-trees-and-sediments

1    **Informative title:** Hydraulic redistribution in mangroves: time-lapse electrical resistivity

2    reveals diel patterns of subsurface salt mobilization consistent with exchange of water

3    between trees and sediments

4    **Running title: Time-lapse electrical resistivity reveals diel patterns of salt mobilization**

5    **Authors:** Christine Downs[1], Sarah Kruse[1]

6    **Affiliations:** [1] University of South Florida, School of Geosciences, 4202 E Fowler Ave,

7    Tampa, FL

15   **Data Availability Statement:** The data that support the findings of this study are available

16   from the corresponding author upon reasonable request. If the journal offers a supplemental

17   repository, the author will make the data available.

18   **Abstract**

19        A 24-hour 2D time-lapse electrical resistivity imaging (ERI) survey was conducted

20   in an altered mangrove forest on a barrier island in southeast Florida, USA, to (1) assess the

21   method's utility in hypersaline conditions and (2) understand how trees respond to

22   hypersaline conditions. ERI measurements serve as a proxy for pore water salinity and

23   saturation. Here, resistivity changes suggest a lag between the tidal cycle and changes in

24   ground resistivity. ERI data show that overall changes within 24 hours are very small, but

25   there is more variability in resistivity in the root zone of mangroves than in open salt flat

26   portions along a fixed transect. Two to three hours after sunset, root zone resistivity

27   increased from initial, midday conditions. Overnight, the root zone was less resistive than

28  midday. By sunrise, root zone resistivity was once again higher than initial conditions.

29  Measurements from the salt flat where roots are absent remained generally constant

30  throughout the survey. Thus, changes in resistivity over time are inferred to reflect

31  mangrove tree physiological influences related to diel water use. A mechanistic

32  explanation for the decreased resistivity two hours after sunset from the re-

33  distribution of salts to the soil around the roots is the Cohesion-Tension Theory,

34  which suggests that trees continue water uptake after sunset to balance the pressure

35  after leaf stomates have closed. The corresponding overnight drop in ground resistivity

36  just prior to sunrise may be explained by redistribution of freshwater from the tree to the

37  soil that was delayed until the early morning hours. The limited period of data acquisition

38  limits definitive data interpretations, but the study illustrates the monitoring potential of

39  ERI in hypersaline environments such as a mangrove forest.

40  **Keywords:** 2D, electrical resistivity, groundwater, mangrove, water uptake

41  **Introduction**

42      Mangrove forests are integral components of tropical and subtropical intertidal

43  forest communities and essential to coastal stabilization and ecological processes. Due to

44  their location between land and sea, mangrove forests play a pivotal role in climate change

45  adaptation and mitigation. They show a great deal of ecological stability (Alongi, 2015)

46  through their ability to elevate land surface via sediment accretion and root zone processes,

47  often on pace with sea-level rise (Krauss et al., 2014; McIvor et al., 2013; McKee et al.,

48  2007, 2012). They also have a strong capacity to act as $CO_2$ sinks (Duarte et al., 2013)

49  while using water conservatively (Lovelock et al., 2006). Their salt tolerance lends

50  mangroves the ability to survive harsh coastal environments (Ball, 1988; Esteban et al.,

51  2013; Parida and Jha, 2010). Some species, like black mangroves (*Avicennia germinans*),

52  rely on foliar salt excretion (Drennan and Pammenter, 1982; Esteban et al., 2013; Parida

53  and Jha, 2010; Scholander et al., 1962) to prevent excess accumulation of  salts not

54  excluded when water was absorbed by roots (though black mangrove trees do filter water at

55  the root). Excreted salt on leaves dissolves during cooler, moister periods and returns to the

56  soil during rain events or via excised leaves. Other species, like red (*Rhizophora mangle*)

57  and white (*Laguncularia racemosa*) mangroves, exclude more salt at the roots. During

58  water uptake, water must move down from the soil surface to the roots. By convection, salt

59  also moves down and is then excluded by roots, thus contributing to a local soil salinity

60  maxima directly in the rhizosphere—the region of soil directly influenced by plant root

61  activity (Passioura et al., 1992). While the salt balance in a given tree is presumably

62  maintained, the subsurface can experience gains in salt concentration over time unless

63  upward diffusion of salt balances the downward convection.

64      Trees may hydrate via foliar absorption of atmospheric water, which can bring more

65  water into the tree than root water uptake alone. This top-down rehydration can ultimately

66  lead to fresh water discharge into the soil. Hao et al. (2009) suggested hydraulic

67  redistribution to explain lower salinities in the root zones of scrub *Rhizophora mangle* that

68  are growing in an area perennially flooded with seawater. Hydraulic redistribution has been

69  demonstrated in many plants of upland ecosystems. Coopman et al. (2021) showed that the

70  capacity of a salt-secreting mangrove (*Avicennia marina*) to access water from an

71  unsaturated atmosphere demonstrates top-down hydration at scales and frequencies of

72  major consequence to tree function under hypersaline conditions. This prompts the

73  questions about the extent and timing of effects of top-down rehydration on soil pore water

74  salinity.

75      Tidal forcing is typically the dominant mechanism of pore water and salt movement

76  in the saturated and intertidal zones of coastal wetlands and can remove locally excess salt

77  caused by mangrove tree activity (Hughes et al., 1998; Sam and Ridd, 1998; Wolanski et

78  al., 1993). However, the construction of impoundments alters the salinity balance

79  maintained under natural conditions, and, globally, mangroves suffer from tidal restrictions

80  that influence their ecological function and sometimes lead to rapid mortality once multiple

81  stress thresholds are exceeded (Lewis et al., 2016). Impoundments can be earthen dikes that

82  surround sections of forest and hydrologically isolate them from tidal surface water and

83  each other, which can lead to concentrated salinities to levels deleterious even to

84  mangroves. In these cases, evapotranspiration (ET) can become the most influential factor

85  in determining pore water salinities and stand stress, particularly during hot, dry periods

86   (Stringer et al., 2010).

87   While the concept of root zone salinity concentration with prolonged daily water
88   uptake and ultrafiltration is theoretically tenable, it is important to document how changes
89   in salinity distribution relate to specific tidal and sunrise/sunset cycles in actual mangrove
90   forests. Transpiration significantly decreases at night when photosynthetically active
91   radiation is eliminated, and air temperatures drop. At this time, the water potential in the
92   roots will rise to slow down or cease the intake of soil water. At the start of the day,
93   transpiration resumes, and the root's water potential drops to facilitate root water uptake.
94   Transpiration in mangroves reaches a maximum rate around midday, but maximum
95   cumulative amounts of water transited each day would be realized slightly after sunset as
96   water uptake continues even after stomates (leaf 'pores') are likely closed (Krauss et al.,
97   2007).

98   This study focuses on an impounded portion of a mangrove forest on a barrier
99   island in east-central Florida, where the forest is isolated from tidal inundation (**Error!**
100  **Reference source not found.**). The impoundment was initially constructed for mosquito
101  abatement. It is comprised of an earthen dike that run along the water's edge and inland to
102  break up the forest into sections. A pump/culvert system is installed within the dike
103  connecting the lagoon to a ditch on the interior side of the dike. In the past, the culvert was
104  a free opening for water to flow through the dike when water levels were high enough.
105  Current water management practices pump brackish water into the impoundment to keep it
106  inundated from April to October to simulate more natural conditions. The impoundment
107  area is then allowed to dry up entirely from November to March.

108  The trees are predominantly black mangroves and most (90%) porewater salt is
109  excluded during water uptake by the roots. The salt that is transported to the shoot either
110  becomes stored for osmotic adjustment or developing tissues. Excess salt is expelled from
111  the leaves via salt excretion glands (Ball et al., 1988). Impoundment practices can decrease
112  mangrove growth rates and diversity (Berrenstein et al., 2013; Brockmeyer Jr et al., 1996;
113  Crase et al., 2013; Harris et al., 2010; Middleton et al., 2008; Rey et al., 2009, 1990; Rey
114  and Rutledge, 2009), which may imply nutrient limitations, prolonged flooding, and soil

115    hypersalinity within the rhizosphere. In fact, it is typically expected that zones with the

116    most active roots have the highest salinity concentrations (Passioura et al., 1991) with

117    levels increasing until the rate of convection transport to the roots equal the rate of diffusive

118    transport to the surface sediment. Stringer and others (2010) hypothesized that, in the

119    impoundment of interest, dense, saline pore water in these active zones sinks to create a

120    hypersaline layer 1-4 m below the mangrove and ecophysiological processes within

121    mangrove vegetation such as hydraulic lift (e.g., Dawson, 1993) interact with this layer to

122    alter salinity concentration within the rhizosphere over a daily transpirational cycle.

123    However, in the absence of mangrove activity as ions diffuse along a concentration gradient

124    toward the soil surface such a hypersaline layer would presumably collapse.

125        We take a geophysical approach to detect spatial and temporal variation in salinity

126    profiles that would reflect diel signatures of water uptake by the trees and hydraulic

127    redistribution of atmospherically-sourced fresh water from the trees into the soil. Time-

128    lapse electrical resistivity imaging (ERI) has proven useful in imaging changes in soil

129    moisture and root uptake (e.g., Beff et al., 2013; Brillante et al., 2016; Consoli et al., 2017;

130    Daily et al., 1992; Garré et al., 2011; Lewis et al., 2016; Mares et al., 2016; Mary et al.,

131    2020; Musgrave and Binley, 2011), the mobility of saline tracers (e.g., Binley et al., 1996;

132    Cassiani et al., 2006; Kemna et al., 2002; Robinson et al., 2020; Singha and Gorelick, 2005;

133    Slater et al., 1997; Slater and Sandberg, 2000) or contaminants (e.g., Hayley et al., 2009;

134    Mansoor and Slater, 2007), and changes in both soil moisture and salinity in saline

135    environments (Attwa et al., 2011; Boaga et al., 2014; Brindt et al., 2019; deFranco et al.,

136    2009; Kiflai et al., 2020; Leroux and Dahlin, 2006; Slater and Sandberg, 2000; Sutter and

137    Ingham, 2016; Urish and Frohlich, 1990; Vacher et al., 2008). This paper reports on the

138    observations made with a time-lapse ERI survey coupled with real-time groundwater data

139    and tidal records. Our objectives were to assess (1) the effectiveness of ERI under

140    hypersaline conditions and (2) the spatiotemporal changes in saline pore water structures as

141    a function of diel and tidal cycles in the absence of surface interaction between the

142    impounded mangrove forest and lagoon. Interpretations were made with consideration

143    given to what is already known about mangrove tree physiological processes in unaltered

144    mangrove forests.

**Field Site**

146     Imp-24 is a mosquito-control impoundment on the west side on North Hutchinson

147     Island, Florida, USA (Figure 1 top). North Hutchinson Island is a siliciclastic barrier island

148     approximately 35 km long and 0.7 km wide. The Indian River Lagoon, a tidal estuarine

149     system, borders the west shore of the island; the Atlantic Ocean borders the east side. The

150     lagoon connects to the Atlantic Ocean about 9 km south of Imp-24, and a lagged and

151     dampened tidal signature is observed in the ditch between the impoundment and the lagoon

152     compared to the semidiurnal tidal regime observed at the lagoon's opening.

153     For the Indian River Lagoon, average precipitation rates are 1,180 mm/yr (Sumner

154     and Belaineh, 2005). Open water evaporation rate is 1,502–1,614 mm/yr, with the lowest

155     rate occurring in the winter months (District, 2006; Sumner and Belaineh, 2005). Vegetated

156     areas experience an estimated 2.6 to 3.5 mm/day (967–1,278 mm/yr) of evapotranspiration

157     based on similar basin mangrove types in the region (Lugo et al., 1975; Twilley and Chen,

158     1998). Mangrove evapotranspiration (ET) rates strongly influence pore water salinities

159     (Esteban et al., 2013), and changes in water management practices in the mangrove forest

160     have also produced changes in the pore water salinity structure. The vegetation and surface

161     water are separated from the neighboring lagoon by an earthen dike. Maximum water levels

162     are maintained during the summer season (~0.6 m, April-October) and allowed to dry

163     during the winter (November-March) (Connelly and Carlson, 2009; Middleton et al., 2008;

164     Rey and Rutledge, 2009). In the dry season, pore water salinities are more heavily affected

165     by ET rates (Stringer et al., 2010), which lowers the water table and creates a gradient that

166     drives lagoon water to the mangrove via groundwater flow (Figure 1 bottom).

167     We established a transect through a high-salinity and small-stature mangrove forest.

168     The very shallow subsurface along the resistivity transect can be partitioned into three

169     vegetative zones (Figure 2 top). From the western end to seven meters along the transect,

170     the surface is dominated by dense, height-restricted scrub mangroves. The central portion is

171     a salt flat with standing roots only along the edges. At the center of the salt flat (about 30 m

172     along the transect), there is a small scrub mangrove patch very near the transect. In a sense,

173     much of the salt flat serves as a control area where the influence from root activity is

174  presumably absent. From 40 m along the transect to the eastern end, the vegetation is

175  characterized by sparse, scrub trees. Digging in the vicinity of trees shows the root zones of

176  dense tree groupings extend as far as 1.5 meters in depth. Shallow sediments are fine-

177  grained sand composed of quartz and calcareous grains (Stringer et al., 2010).

178  **Methods**

179      With an AGI Supersting R8 resistivity meter, we performed repeated electrical

180  surveys over 24 hours (March 27–28, 2015) at the end of the "dry" season. Fifty-six

181  electrodes remained stationary throughout the survey. It was important to have high lateral

182  sensitivity in the root zone (0-2 m depth) and moderate vertical sensitivity in the top two

183  meters. Thus, a combined dipole-dipole inverse Schlumberger array configuration with a 1-

184  meter dipole spacing was chosen. Each survey took approximately 45 minutes. To capture

185  both diel and tidal effects on salinity structures in the sub-surface, a 2-D transect array was

186  collected approximately every hour for 24 hours starting at about noon on day 1. Gaps exist

187  in our acquisition schedule due to battery issues. Nevertheless, there is at least one data set

188  representing four diel-tidal combinations—daytime, low tide; daytime, high tide; nighttime,

189  low tide; nighttime, high tide. The first survey acquired 1219 quadripoles; subsequent

190  surveys collected 1045 to 1146 quadripoles for a total of 13,890.

191      There was standing water at certain times on the western half of the array, so

192  electrodes were cased in PVC pipes pushed approximately 3 cm into the ground to avoid

193  losing current to surface water. Contact resistance tests confirmed the ground was wet

194  enough to deem watering the electrodes with saltwater unnecessary. Relief along the

195  transect, as observed in a LiDAR-derived digital elevation model, is extremely subtle (0.07

196  m). For this reason, topography was not included in the inversion.

197      As in any ER study, it is necessary to assess measurement error before data

198  inversion and interpretation. Following the repeat measurement error assessment of Brindt

199  et al. (2019) and Mares et al. (2016), for example, measurements with an acquisition error

200  above 2% were removed (Figure 2 bottom). Of the 13,890 quadripoles collected, 13,573

201  were used in the inversion.

202    The resistivity data were inverted with ResIPy, an open-source geoelectric inversion

203    and modeling software (Blanchy et al., 2020). The models were parameterized on a

204    triangular mesh with the finest node spacing closest to the surface (~0.25 m) and

205    progressively coarser spacing (~1 m) with depth. The first time step was inverted using a

206    uniform reference model of 100 Ωm. Time-lapse inversion is preferred because outliers or

207    noise inherent in each dataset has less influence in the solution versus individual solutions

208    (Binley et al., 1996; Loke, 2014). Time steps were regularized relative to the first dataset to

209    prioritize smoothing changes from one dataset to the next. When the inversion was

210    complete, data points that had a misfit beyond ±3% were filtered out, and the data were

211    inverted again.

212    Direct groundwater data were also collected using Decagon conductivity,

213    temperature, and water depth sensors (CTD) deployed down PVC wells. The PVC wells,

214    installed four months earlier, were screened at 0.6 m and 1.2 m and resided at the western

215    edge of the transect. Sensors were calibrated at the start of the first day of sampling with

216    room temperature with tap water. The sensors recorded measurements at 15-minute

217    intervals throughout the ERI survey. Due to equipment failure, only water conductivity and

218    one set of temperature readings are presented.

219    **Results and Discussion**

220    The depth of investigation (DOI) was assessed using the method described by

221    Oldenburg and Li (1999), where the first time step is inverted using two different reference

222    resistivities (0.06 and 5.69 Ωm). These reference values were based on the average

223    observed apparent resistivity values. Considering a cautious DOI index cutoff of 0.1, our

224    maximum depth of investigation is about 5 m with the exception of the first 2 m along the

225    array. The true resolution matrix (Figure 3) (Binley and Kemna, 2005, Eq. 5.18) shows

226    inverted resistivity is best resolved in the first 1-2 meters, which is suitable for imaging

227    changes in the root zone of mangrove trees. Accordingly, only the top 2 m of resistivity

228    profiles are presented and discussed.

229    The inversion results yield zones with near-electrode values that locally alternate

230    between relatively high and low resistivity, particularly at electrodes placed in between tree

231    roots. This is likely due to noisy data as a result of poor contact between electrodes and

232    sediment. Since noise appears to be an issue in vegetated zones and not the open salt plan,

233    the roots themselves may contribute to poor electrode contact. Small burrowing animals

234    (e.g., fiddler crabs; Ocypodidae) are common in the forest and the distribution of their

235    burrows, which would contribute to poor contact, may be concentrated in the root zone. It is

236    also worth noting that burrowing animal activity also alters local mud chemistry due to

237    enhanced diffusive exchange of dissolved material between the surface and porewater

238    through the sediment surface (Smith et al., 1991).

239    Since inversion results suffer from near-electrode artifacts, and reciprocal readings

240    were not collected due to time constraints , we present first-order trends and patterns

241    between time-lapse inversion results and environmental changes as measured in ancillary

242    data. Terrain resistivity is controlled by temperature, ground saturation, matrix properties,

243    and groundwater salinity. Results are presented in terms of change from the first time step,

244    thus removing the signature of presumably static matrix properties. The remaining

245    parameters are discussed in turn.

246    The ground temperature at 0.6 m depth was 22° C at the start of the survey and

247    decreased to 21° C by the end of the survey (Figure 4 bottom). This temperature decrease

248    corresponds to a 2% apparent resistivity increase, which is small but so are resistivity

249    changes between time steps. We use the linear temperature-dependent model from Hayley

250    et al. (2007) and the fractional change coefficient (m=0.0187) by Hayashi (2004) to

251    calculate the effect of groundwater temperature at 0.6 m on electrical resistivity

252    measurements. Ground temperature was measured at 15-minute intervals. For a given ERI

253    time step, we averaged ground temperature measurements collected over the duration of a

254    given ERI acquisition time. The temperature-dependent model was applied to each ERI

255    time step using these average values and 22°C as the standard value.

256    Terrain resistivity is expected to be inversely proportional to the degree of

257    groundwater saturation (e.g., Archie, 1942). There were approximately 4 cm of standing

258    water at the western end of the transect at the start of the study. Surface water levels along

259    this western end gradually dropped until there was no standing water, and did not return

260    through the course of the 24-hour recording period, as would have been expected had the

261    local surface water levels tracked the tidal cycle recorded at the pump station in the trench

262    between the earthen dike and mangrove forest (Locer, 2016) (Figure 4 top). The portion of

263    the forest where the survey took place is thus far enough inland to have not been

264    completely inundated during high tide, and the saturation pattern is not readily correlated

265    with tides. It had rained 18 hours before the study, and standing water levels might also

266    reflect local lateral surface water perching and flow. The ground appeared highly saturated

267    throughout to the end of the study, in the sense that augered holes showed full saturation at

268    depths less than 10 cm.

269       Pore water resistivity at 0.6 m depth and 1.2 m depth are compared with the mean

270    apparent resistivity from the top 2 meters and easternmost 5 meters along the ERI transect

271    of each time step (Figure 4, middle and bottom, respectively). The ranges of measurement

272    values from 0.6 m and 1.2 m depths are 0.15-0.18 $\Omega$m and 0.12-0.13 $\Omega$m, respectively.

273    This is a narrower range than that of apparent resistivities (0.01 – 9.23 $\Omega$m) from the west

274    end of the profile. A formation factor is the ratio of the resistivity of water-filled rock or

275    sediment to that of the water and is often used to describe porosity or at least expected

276    porosity for a given geomaterial  (Archie, 1942). An average formation factor is estimated

277    here by taking the ratio between water resistivity at 0.6 m depth and the inverted resistivity

278    value for the model cells closest to the location of the 0.6 m well at the east end of the

279    array. Both groundwater conductivity and inverted terrain resistivity were averaged over

280    the diel period, to yield a formation factor of 4.8. This differs from the previous estimate of

281    3.6 by Stringer et al. (2010), which was based on electromagnetic measurements of terrain

282    conductivity with larger sampling volumes. It has been shown that the formation factor

283    varies spatially and temporally (Singha and Gorelick, 2005), so it is reasonable—and

284    expected—to resolve a range of values at a local scale. The 4.8 value is within the range of

285    published formation factors for sandy soils, such as found at the study site.

286       Temporal variations in pore water conductivity recorded over the diel period at the

287    wells at 0.6 m and 1.2 m are quite small and not synchronous (Figure 5, middle and

10

288  bottom). Measurements (converted from conductivity to resistivity for comparative

289  purposes) at 0.6 m correspond to salinities between 38 and 41 psu (Fofonoff and Millard,

290  1983). Measurements at 1.2 m correspond to above-seawater salinities and are beyond the

291  range of valid values for converting to salinity. The sum of apparent resistivity from each

292  time step is compared to air temperature as well (Figure 5), which helps make inferences

293  about the relationship between ground salinity and saturation and factors that influence ET.

294  Resistivity values for the entire time-lapse survey range from 0.13 to 2600 Ωm. The median

295  resistivity is 2.8 Ωm; the standard deviation is 1.6 Ωm. Figure 6 shows the change a

296  resistivity between a given time step and the first time step. The values between time steps

297  are quite noisy, as they are relatively small compared to the overall signature. In this study,

298  we focus on first-order trends as they relate to diel and tidal stages within the vegetation

299  zone.

300  ### *Root zone*

301  　　　　Overall, the root zones are more resistive than the neighboring salt flat as expected

302  as roots ameliorate salinity conditions (Figure 6, left column). This applies to the tree

303  groupings on the east and west ends of the resistivity profile and the single shrub in the

304  middle of the profile (Figure 2 top). The patch of standing roots extending out from the

305  western tree grouping away from the forest canopy to about 15 m along the transect is

306  also consistently more resistive than the rest of the salt flat.

307  　　　　We present the difference in inverted resistivity between selected time steps and the

308  initial model at 13:00 during a rising tide (Figure 6, right column). The median difference

309  from the initial model (for all time steps) is 0.22 Ωm, the interquartile range is 0.47 Ωm,

310  and the standard deviation is 1.69 Ωm. Outliers concentrated near selected electrodes are

311  likely due to loss of contact between the electrode and the soil. These values are not shown

312  in Figure 6.

313  　　　　The western tree grouping, including the standing roots extending 15 m into the salt

314  flat, experienced an increase in resistivity (0.5 to 1.3 Ωm increase) from the afternoon until

315  after sunset (22:00) when the tide was falling. This portion of the profile  then becomes

316  progressively less resistive until 03:30 (rising tide) when the area is 0.5 to 2 Ωm less

317  resistive than the initial state. From 05:00 to 07:00, conditions are essentially the same as

318  the initial state. After sunrise (08:00 to11:00), the western tree grouping and standing roots

319  are once again more resistive than the initial conditions though not to the same extent as the

320  previous afternoon and evening.

321      The single shrub in the middle of the salt flat presents a similar trend. Conditions

322  are more resistive than the initial state through the afternoon and early evening. Resistivity

323  decreases until the early morning hours when conditions are similar to or less resistive than

324  the initial state. The area is once again more resistive after sunrise. The eastern tree

325  grouping consistently yields very large changes from the initial model. Although outliers

326  are present, the overall trend suggests the area is more resistive than initial conditions

327  during the day and less resistive overnight.

328  **Interpretations**

329      The temporal changes in the resistivity profiles are on the same scale as those in the

330  measured groundwater conductivities over the diel period (Figure 4); however, they do not

331  necessarily follow the same trend. Such small changes in ground conductivities, as

332  measured in the ER data, fall in the envelope of instrument error ($\pm0.01$ mS/cm or $\pm$1e3

333  Ωm.)  The overall values do yield a plausible formation factor, and the higher pore water

334  resistivities recorded at 0.6-meter depth over those at 1.2-meters depth agree with the

335  distribution recorded in the resistivity surveys. The terrain resistivity data are robust in that

336  they agree with the observed geological structure and show general trends that can be

337  interpreted.

338      In a coastal environment, one can expect shallow terrain resistivities to be their

339  lowest at high tide when tidal forcing increases the extent of brackish water ingress.

340  Although the impoundment does not experience tidal inundation, we considered any

341  signature of tidal forcing. In this study, the lowest resistivities are observed overnight after

342  high tide as the tide is falling (Figure 4; Figure 6, right column). This would indicate that

343  the tidal cycle does influence ground resistivity and that there is a time lag between high

12

344     tide and minimum ground resistivity. On the other hand, the same pattern is not observed

345     before sunset when the tide is also falling. Furthermore, this pattern is not captured by

346     direct groundwater measurements. Thus, our observations do not appear to support tidal

347     cycles as the sole controller of the observed resistivity cycle.  We consider instead that our

348     ER data are, at least partially, controlled by pore water conductivity and saturation changes,

349     which are, to some extent, controlled by tree activity and varies with the time of day.

350        Low water pressure potential in roots creates an upward hydraulic gradient during

351     daylight hours. Black mangrove trees partially filter salts at the root during water uptake

352     and excrete excess salt from the leaves during transpiration. Transpiration rates of south

353     Florida mangrove trees slow down with stomatal closure at sundown, but upward stem

354     water movement (sap flow) continues one to two hours in many tree species after sunset

355     as continued water absorption is required for rehydration of tissues in an effort to balance

356     the pressure well after stomates are closed (Meinzer et al., 2004). Black mangroves

357     growing in scrub environments of Louisiana, USA continue to take water up for at least an

358     hour or more after sunset (Krauss et al., 2014). The water pressure gradient in a tree is

359     inversely proportional to its water content. Accordingly, the sustained upward sap flow can

360     continue until the pressure gradient between soil pore water and the tree collapses.

361     Recharge of the soil possible if the tree achieves a higher water potential than that of pore

362     water around the roots. A possible scenario for this could be the uptake of water from roots

363     at shallow soil depths where pore water salinity is lower than that of soil pore water

364     surrounding roots at greater soil depths. This may lead to a downward transfer, via reverse

365     sap flow, of low salinity water extracted from shallow soil depths and transported through

366     the tree into greater soil depths. Whether reverse sap flow occurs or not, transpiration

367     resumes at sunrise prompting the upward hydraulic gradient once again.

368        If we consider this cycle in terms of the resistivity results, some patterns emerge.

369     Relative to the first time step at 15:00, the root zone became more resistive in the late

370     afternoon before sunset (Figure 6, right column). These conditions continued— though a

371     slight decrease in resistivity is present after sunset (19:30)— until approximately midnight.

372     Recall that black mangrove trees exclude 90% of pore water salts during water uptake. We

373    attribute the increased resistivity to continual water uptake of filtered water stranding

374    salts in the rhizosphere, suggesting the ER response is from a combination of declining

375    water content and increased soil salinity. The trend continues throughout the first half of the

376    night as sap flow is known to also continue. Boaga et al. (2014), for example, also show

377    that water uptake in the root zone can produce pockets of more resistive ground even when

378    the surface is flooded.

379        From about midnight to sunrise, the ground is overall less resistive than initial

380    conditions. The largest decreases occurring in vegetated areas. The salt flat is only slightly

381    less resistive than initial conditions (about -0.25 $\Omega$m) and the change is very uniform. In a

382    sense, the salt flat where roots are completely absent serve as a control area. We attribute

383    the larger decrease in resistivity to water uptake ceasing and even freshwater recharge to

384    the area around trees via reverse sap flow (e.g. Coopman et al., 2021).  Again, this suggests

385    that varying water content is driving the ER signal.

386        Ground conditions are once again more resistive than initial conditions by sunrise

387    (07:30). The pattern in increased resistivity is similar to that pre-sunset with the most

388    significant changes occurring in vegetated and standing root areas. These conditions

389    continue through to the end of the survey (11:00). We attribute this to transpiration

390    resuming, prompting an upward hydraulic gradient and water uptake.

391        The suggestion of water returning to the soil via tree roots is the process known as

392    hydraulic redistribution that has been observed in dry environments (Caldwell et al., 1998;

393    Caldwell and Richards, 1989; Ludwig et al., 2003; Richards and Caldwell, 1987),

394    temperate forests (Meinzer et al., 2004), savannas (Meinzer et al., 2004; Scholz et al., 2002)

395    and mangrove forests (Hao et al., 2009). Hao and others (2009) found that reverse flow in

396    dwarf red mangroves in south Florida may help to relieve the adverse effects of hypersaline

397    conditions in a given tree. Our results support this process. While the hypersaline

398    conditions in the impounded mangrove forest discuss here are detrimental to mangrove tree

399    growth, hydraulic redistribution may be an important factor in addition to salt exclusion and

400    salt excretion for its survival (Figure 7).

401        The mangrove trees may then reverse their pressure gradient overnight rather than

402    simply reduce water uptake completely and redistribute freshwater to the root zone slowly

403    thereafter, perhaps in combination with high tide. Such a phenomenon would indicate

404    mangrove trees benefit from hydraulic redistribution overnight to offset maximum

405    transpiration-imposed root zone salinity increases by the end of the day and into the early

406    part of the evening. This would require an alternative source of water, specifically uptake of

407    atmospheric water.

408        Our study tests the ability of electrical resistivity to detect small changes in ground

409    resistivity in a hypersaline environment. The observations presented here are temporally

410    finite. It is not possible to make inferences about seasonal or annual patterns or even

411    average daily processes. Nevertheless, the data indicate a tidal influence compounded with

412    mangrove tree physiological processes, understanding of which ultimately assists in

413    assessing the long-term effects of diking on mangrove forests.

414    **Conclusions**

415        We evaluate the use of repeat electrical resistivity surveys to image changing

416    ground conditions in a hypersaline mangrove environment.  Time-lapse electrical resistivity

417    surveys capture dynamic processes within the root zone of a mangrove forest over a diel

418    cycle and appear to reflect tree physiological processes and tidal forcing. We infer that the

419    mangrove trees in an impounded forest on a barrier island may pull saline water up from

420    the root zone during the day and for a time after sunset. The data suggest that this process

421    reverses overnight when fresher water is returned to the soil via hydraulic redistribution.

422    The period over which data acquisition took place limits data interpretations and the data

423    appears to suffer from noise due to questionable contact between electrodes and sediment.

424    Nevertheless, this study presents the utility of ER in monitoring plant-soil interactions in

425    hypersaline environments, such as a mangrove forest.

426    **References**

427    Alongi, D.M., 2015. The impact of climate change on mangrove forests. Curr. Clim.

428        Chang. Reports 1, 30–39.

429    Archie, G.E., 1942. The electrical resistivity log as an aid in determining some reservoir
430        characteristics. Trans. AIME 146, 54–62.

431    Attwa, M., Günther, T., Grinat, M., Binot, F., 2011. Evaluation of DC, FDEM and IP
432        resistivity methods for imaging perched saltwater and a shallow channel within coastal
433        tidal flat sediments. J. Appl. Geophys. 75, 656–670.
434        https://doi.org/10.1016/j.jappgeo.2011.09.002

435    Ball, M.C., 1988. Ecophysiology of mangroves. Trees 2, 129–142.

436    Beff, L., Günther, T., Vandoorne, B., Couvreur, V., Javaux, M., 2013. Three-dimensional
437        monitoring of soil water content in a maize field using electrical resistivity
438        tomography. Hydrol. Earth Syst. Sci. 17. https://doi.org/10.5194/hess-17-595-2013

439    Berrenstein, H.J., Mans, D.R.A., Bhansing, M., Wakiran, W.S., Atmopawiro, S.L.,
440        Chotkan, N.R., Karsoredjo, R.S., Sabiran, S.A., 2013. Effects of diking on the
441        biological performance of the black mangrove (Avicennia germinans L.) in an Atlantic
442        mangrove forest. Wetl. Ecol. Manag. 21, 165–172.

443    Binley, A., Henry-Poulter, S., Shaw, B., 1996. Examination of solute transport in an
444        undisturbed soil columnusing electrical resistance tomography. Water Resour. Res. 32,
445        763–769.

446    Binley, A., Kemna, A., 2005. DC Resistivity and Induced Polarization Methods, in:
447        Hydrogeophysics. https://doi.org/10.1007/1-4020-3102-5_5

448    Blanchy, G., Saneiyan, S., Boyd, J., McLachlan, P., Binley, A., 2020. ResIPy, an intuitive
449        open source software for complex geoelectrical inversion/modeling. Comput. Geosci.
450        https://doi.org/10.1016/j.cageo.2020.104423

451    Boaga, J., D'Alpaos, A., Cassiani, G., Marani, M., Putti, M., 2014. Plant-soil interactions in
452        salt marsh environments: Experimental evidence from electrical resistivity
453        tomography in the Venice Lagoon. Geophys. Res. Lett. 41.
454        https://doi.org/10.1002/2014GL060983

455    Brillante, L., Bois, B., Mathieu, O., Lévêque, J., 2016. Electrical imaging of soil water

456       availability to grapevine: a benchmark experiment of several machine-learning

457       techniques. Precis. Agric. 17. https://doi.org/10.1007/s11119-016-9441-1

458 Brindt, N., Rahav, M., Wallach, R., 2019. ERT and salinity – A method to determine

459       whether ERT-detected preferential pathways in brackish water-irrigated soils are

460       water-induced or an artifact of salinity. J. Hydrol. 574.

461       https://doi.org/10.1016/j.jhydrol.2019.04.029

462 Brockmeyer Jr, R.E., Rey, J.R., Virnstein, R.W., Gilmore, R.G., Earnest, L., 1996.

463       Rehabilitation of impounded estuarine wetlands by hydrologic reconnection to the

464       Indian River Lagoon, Florida (USA). Wetl. Ecol. Manag. 4, 93–109.

465 Caldwell, M.M., Dawson, T.E., Richards, J.H., 1998. Hydraulic lift: consequences of water

466       efflux from the roots of plants. Oecologia 113, 151–161.

467 Caldwell, M.M., Richards, J.H., 1989. Hydraulic lift: water efflux from upper roots

468       improves effectiveness of water uptake by deep roots. Oecologia 79, 1–5.

469 Cassiani, G., Bruno, V., Villa, A., Fusi, N., Binley, A., 2006. A saline trace test monitored

470       via time-lapse surface electrical resistivity tomography. J. Appl. Geophys. 59, 244–

471       259.

472 Connelly, C.R., Carlson, D.B. (Eds.), 2009. Florida Mosquito Control: The state of the

473       mission as defined by mosquito controllers, regulators, and environmental managers.,

474       Florida Co. ed. University of Florida, Institute of Food and Agriculture Sciences,

475       Florida Medical Entomology Laboratory, Vero Beach, FL.

476 Consoli, S., Stagno, F., Vanella, D., Boaga, J., Cassiani, G., Roccuzzo, G., 2017. Partial

477       root-zone drying irrigation in orange orchards: Effects on water use and crop

478       production characteristics. Eur. J. Agron. https://doi.org/10.1016/j.eja.2016.11.001

479 Coopman, R.E., Nguyen, H.T., Mencuccini, M., Oliveira, R.S., Sack, L., Lovelock, C.E.

480       and Ball, M.C., 2021. Harvesting water from unsaturated atmospheres: deliquescence

481       of salt secreted onto leaf surfaces drives reverse sap flow in a dominant arid climate

482       mangrove, Avicennia marina. New Phytologist, *231*(4), pp.1401-1414.

483    Crase, B., Liedloff, A., Vesk, P.A., Burgman, M.A., Wintle, B.A., 2013. Hydroperiod is the
484          main driver of the spatial pattern of dominance in mangrove communities. Glob. Ecol.
485          Biogeogr. 22, 806–817.

486    Daily, W., Ramirez, A., LaBrecque, D., Nitao, J., 1992. Electrical resistivity tomography of
487          vadose water movement. Water Resour. Res. 28, 1429–1442.
488          https://doi.org/10.1029/91WR03087

489    Dawson, T.E., 1993. Hydraulic lift and water use by plants: implications for water balance,
490          performance and plant-plant interactions. Oecologia 95.
491          https://doi.org/10.1007/BF00317442

492    deFranco, R., Biella, G., Tosi, L., Teatini, P., Lozej, A., Chiozzotto, B., Giada, M.,
493          Rizzetto, F., Claude, C., A., M., and Bassan, V., Gasparetto-Stori, G., 2009.
494          Monitoring the saltwater intrusion by time lapse electrical resistivity tomography: The
495          Chioggia test site (Venice Lagoon, Italy). J. Appl. Geophys. 69, 117–130.
496          https://doi.org/10.1016/j.jappgeo.2011.08.004

497    District, S.J.R.W.M., 2006. Evaluation of potential impact of demineralization
498          concentration discharge to the Indian River Lagoon (study).

499    Drennan, P., Pammenter, N.W., 1982. Physiology of salt excretion in the mangrove
500          Avicennia marina (Forsk.) Vierh. New Phytol. 91, 597–606.

501    Duarte, C.M., Losada, I.J., Hendriks, I.E., Mazarrasa, I., Marbà, N., 2013. The role of
502          coastal plant communities for climate change mitigation and adaptation. Nat. Clim.
503          Chang. 3. https://doi.org/10.1038/NCLIMATE1970

504    Esteban, R., Fernández-Marìn, B., Hernandez, A., Jiménez, E.T., León, A., Garcìa-
505          Mauriño, S., Silva, C.D., Dolmus, J.R., Dolmus, C.M., Molina, M.J., Others, 2013.
506          Salt crystal deposition as a reversible mechanism to enhance photoprotection in black
507          mangrove. Trees 27, 229–237.

508    Fofonoff, N.P., Millard, R.C., 1983. Algorithms for computation of fundamental properties
509          of seawater. UNESCO Tech. Pap. Mar. Sci. 44. https://doi.org/10.1111/j.1365-

510       2486.2005.001000.x

511   Garré, S., Javaux, M., Vanderborght, J., Pagès, L., Vereecken, H., 2011. Three-dimensional
512       electrical resistivity tomography to monitor root zone water dynamics. Vadose Zo. J.
513       https://doi.org/10.2136/vzj2010.0079

514   Hao, G.-Y., Jones, T.J., Luton, C., Zhang, Y.-J., Manzane, E., Scholz, F.G., Bucci, S.J.,
515       Cao, K.-F., Goldstein, G., 2009. Hydraulic redistribution in dwarf Rhizophora mangle
516       trees driven by interstitial soil water salinity gradients: impacts on hydraulic
517       architecture and gas exchange. Tree Physiol. 29, 697–705.

518   Harris, R.J., Milbrandt, E.C., Everham III, E.M., Bovard, B.D., 2010. The effects of
519       reduced tidal flushing on mangrove structure and function across a disturbance
520       gradient. Estuaries and coasts 33, 1176–1185.

521   Hayashi, M., 2004. Temperature-electrical conductivity relation of water for environmental
522       monitoring and geophysical data inversion. Environ. Monit. Assess. 96, 119–128.
523       https://doi.org/10.1023/B:EMAS.0000031719.83065.68

524   Hayley, K., Bentley, L.R., Gharibi, M., 2009. Time-lapse electrical resistivity monitoring
525       of salt-affected soil and groundwater. Water Resour. Res. 45.
526       https://doi.org/10.1029/2008WR007616

527   Hayley, K., Bentley, L.R., Gharibi, M., Nightingale, M., 2007. Low temperature
528       dependence of electrical resistivity: Implications for near surface geophysical
529       monitoring. Geophys. Res. Lett. 34.

530   Hughes, C.E., Binning, P., Willgoose, G.R., 1998. Characterisation of the hydrology of an
531       estuarine wetland. J. Hydrol. 211, 34–49.

532   Kemna, A., Vanderborght, J., Kulessa, B., Vereecken, H., 2002. Imaging and
533       characterisation of subsurface solute transport using electrical resistivity tomography
534       ERT and equivalent transport models. J. Hydrol. 267, 125–146.

535   Kiflai, M.E., Whitman, D., Ogurcak, D.E., Ross, M., 2020. The Effect of Hurricane Irma
536       Storm Surge on the Freshwater Lens in Big Pine Key, Florida using Electrical

537      Resistivity Tomography. Estuaries and Coasts 43. https://doi.org/10.1007/s12237-019-
538      00666-3

539    Krauss, K.W., McKee, K.L., Lovelock, C.E., Cahoon, D.R., Saintilan, N., Reef, R., Chen,
540      L., 2014. How mangrove forests adjust to rising sea level. New Phytol. 202, 19–34.

541    Krauss, K.W., Young, P.J., Chambers, J.L., Doyle, T.W., Twilley, R.R., 2007. Sap flow
542      characteristics of neotropical mangroves in flooded and drained soils. Tree Physiol.
543      27, 775–783.

544    Leroux, V., Dahlin, T., 2006. Time-lapse resistivity investigations for imaging saltwater
545      transport in glaciofluvial deposits. Environ. Geol. 49, 347–358.
546      https://doi.org/10.1007/s00254-005-0070-7

547    Lewis, R.R., Milbrandt, E.C., Brown, B., Krauss, K.W., Rovai, A.S., Beever, J.W., Flynn,
548      L.L., 2016. Stress in mangrove forests: Early detection and preemptive rehabilitation
549      are essential for future successful worldwide mangrove forest management. Mar.
550      Pollut. Bull. 109. https://doi.org/10.1016/j.marpolbul.2016.03.006

551    Locer, E., 2016. Locer Environmental [WWW Document]. URL
552      http://data.locherenv.com/vdv/index.php

553    Loke, M.H., 2014. Time-lapse resistivity imaging inversion, in: 5th EEGS-ES Meeting.
554      https://doi.org/10.3997/2214-4609.201406397

555    Lovelock, C.E., Ball, M.C., Feller, I.C., Engelbrecht, B.M.J., Ewe, M.L., Ling Ewe, M.,
556      2006. Variation in hydraulic conductivity of mangroves: influence of species, salinity,
557      and nitrogen and phosphorus availability. Physiol. Plant. 127, 457–464.

558    Ludwig, F., Dawson, T.E., de Kroon, H., Berendse, F., Prins, H.H.T., 2003. Hydraulic lift
559      in Acacia tortilis trees on an East Africansavanna. Oecologia 134, 293–300.

560    Lugo, A.E., Evink, G., Brinson, M.M., Broce, A., Snedaker, S.C., 1975. Diurnal rates of
561      photosynthesis, respiration, and transpiration in mangrove forests of south Florida, in:
562      Golley, F.B., Medina, E. (Eds.), Tropical Ecological Systems, Vol. 11. Springer, pp.

563      335–350. https://doi.org/https://doi.org/10.1007/978-3-642-88533-4_22

564    Mansoor, N., Slater, L., 2007. Aquatic electrical resistivity imaging of shallow-water

565      wetlands. Geophysics 72, F211–F221.

566    Mares, R., Barnard, H.R., Mao, D., Revil, A., Singha, K., 2016. Examining diel patterns of

567      soil and xylem moisture using electrical resistivity imaging. J. Hydrol. 536.

568      https://doi.org/10.1016/j.jhydrol.2016.03.003

569    Mary, B., Peruzzo, L., Boaga, J., Cenni, N., Schmutz, M., Wu, Y., Hubbard, S.S., Cassiani,

570      G., 2020. Time-lapse monitoring of root water uptake using electrical resistivity

571      tomography and mise-à-la-masse: a vineyard infiltration experiment. SOIL 6, 95–114.

572      https://doi.org/10.5194/soil-6-95-2020

573    McIvor, A.L., Spencer, T., Möller, I., Spalding, M., 2013. The response of mangrove soil

574      surface elevation to sea level rise. Nat. Coast. Prot. Ser. Rep. 3. CambridgeCoastal

575      Res. Unit Work. Pap. 42. ISSN 2050-7941.

576    McKee, K., Rogers, K., Saintilan, N., 2012. Response of salt marsh and mangrove wetlands

577      to changes in atmospheric CO2, climate, and sea level, in: Global Change and the

578      Function and Distribution of Wetlands. https://doi.org/10.1007/978-94-007-4494-3_2

579    McKee, K.L., Cahoon, D.R., Feller, I.C., 2007. Caribbean mangroves adjust to rising sea

580      level through biotic controls on change in soil elevation. Glob. Ecol. Biogeogr. 16.

581      https://doi.org/10.1111/j.1466-8238.2007.00317.x

582    Meinzer, F.C., Brooks, J.R., Bucci, S., Goldstein, G., Scholz, F.G., Warren, J.M., 2004.

583      Converging patterns of uptake and hydraulic redistribution of soil water in contrasting

584      woody vegetation types. Tree Physiol. 24, 919–928.

585    Middleton, B., Devlin, D., Proffitt, E., McKee, K., Cretini, E.F., 2008. Characteristics of

586      mangrove swamps managed for mosquito control in eastern Florida, USA. Mar. Ecol.

587      Prog. Ser. 371, 117–129.

588    Musgrave, H., Binley, A., 2011. Revealing the temporal dynamics of subsurface

589      temperature in a wetland using time-lapse geophysics. J. Hydrol. 396.

590       https://doi.org/10.1016/j.jhydrol.2010.11.008

591   Oldenburg, D.W., Li, Y., 1999. Estimating depth of investigation in DC resistivity and IP
592       surveys. Geophysics 64, 403–416. https://doi.org/10.1190/1.1444545

593   Parida, A.K., Jha, B., 2010. Salt tolerance mechanisms in mangroves: A review. Trees 24,
594       199–217.

595   Passioura, J. B., M. C. Ball, and J. H. Knight. 1992. Mangroves may salinize the soil and in
596       so doing limit their transpiration rate. Functional Ecology. 6, 4, 476-481.
597       https://doi.org/10.2307/2389286

598   Rada, F., Goldstein, G., Orozco, A., Montilla, M., Zabala, O., Azocar, A., 1989. Osmotic
599       and turgor relations of three mangrove ecosystem species. Funct. Plant Biol. 16, 477–
600       486.

601   Rey, J.R., O'Connell, S.M., Carlson, D.B., Brockmeyer Jr, R.E., 2009. Characteristics of
602       mangrove swamps managed for mosquito control in eastern Florida, USA: a re-
603       examination. Mar. Ecol. Prog. Ser. 389, 295–300.

604   Rey, J.R., Rutledge, C.R., 2009. Mosquito Control Impoundments. Entomol. Nematol.

605   Rey, J.R., Shaffer, J., Crossman, R., Tremain, D., 1990. Above-ground primary production
606       in impounded, ditched, and natural Batis-salicornia marshes along the Indian River
607       Lagoon, Florida, USA. Wetlands 10, 151–171.

608   Richards, J.H., Caldwell, M.M., 1987. Hydraulic lift: substantial nocturnal water transport
609       between soil layers by Artemisia tridentata roots. Oecologia 73, 486–489.

610   Robinson, J., Buda, A., Collick, A., Shober, A., Ntarlagiannis, D., Bryant, R., Folmar, G.,
611       Andres, S., Slater, L., 2020. Electrical monitoring of saline tracers to reveal subsurface
612       flow pathways in a flat ditch-drained field. J. Hydrol.
613       https://doi.org/10.1016/j.jhydrol.2020.124862

614   Sam, R., Ridd, P., 1998. Spatial variations of groundwater salinity in a mangrove-salt flat
615       system, Cocoa Creek, Australia. Mangroves Salt Marshes 2, 121–132.

616 Scholander, P.F., Hammel, H.T., Hemmingsen, E., Garey, W., 1962. Salt balance in

617       mangroves. Plant Physiol. 37, 722.

618 Scholz, F.G., Bucci, S.J., Guillermo, G., and Meinzer, F.C., Franco, A.C., 2002. Hydraulic

619       redistribution of soil water by neotropical savanna trees. Tree Physiol. 22, 603–612.

620 Singha, K., Gorelick, S.M., 2005. Saline tracer visualized with three-dimensional electrical

621       resistivity tomography: Field-scale spatial moment analysis. Water Resour. Res.

622       https://doi.org/10.1029/2004WR003460

623 Slater, L., Binley, A.M., Daily, W., Johnson, R., 2000. Cross-hole electrical imaging of a

624       controlled saline tracer injection. J. Appl. Geophys. https://doi.org/10.1016/S0926-

625       9851(00)00002-1

626 Slater, L., Zaidman, M.D., Binley, A.M., West, L.J., 1997. Electrical Imaging of Saline

627       Tracer Migration for the Investigation of Unsaturated Zone Transport Mechanisms.

628       Hydrol. Earth Syst. Sci. https://doi.org/10.5194/hess-1-291-1997

629 Slater, L.D., Sandberg, S.K., 2000. Resistivity and induced polarization monitoring of salt

630       transport under natural hydraulic gradients. GEOPHYSICS.

631       https://doi.org/10.1190/1.1444735

632 Smith III, T.J., Boto, K.G., Frusher, S.D. and Giddins, R.L., 1991. Keystone species and

633       mangrove forest dynamics: the influence of burrowing by crabs on soil nutrient status

634       and forest productivity. Estuarine, coastal and shelf science, *33*(5), pp.419-432.

635 Stringer, C.E., Rains, M.C., Kruse, S., Whigham, D., 2010. Controls on water levels and

636       salinity in a barrier island mangrove, Indian River Lagoon, Florida. Wetlands 30, 725–

637       734.

638 Sumner, D.M., Belaineh, G., 2005. Evaporation, precipitation, and associated salinity

639       changes at a humid, subtropical estuary. Estuaries 28, 844–855.

640 Sutter, E., Ingham, M., 2016. Seasonal saline intrusion monitoring of a shallow coastal

641       aquifer using time-lapse DC resistivity traversing. Near Surf. Geophys. 14, 1–15.

642       https://doi.org/10.3997/1873-0604.2016039

643 Twilley, R.R., Chen, R., 1998. A water budget and hydrology model of a basin mangrove
644     forest in Rookery Bay, Florida. Mar. Freshw. Res. 49, 309–323.

645 Urish, D.W., Frohlich, R.K., 1990. Surface electrical resistivity in coastal groundwater
646     exploration. Geoexploration 26, 267–289.

647 Vacher, H.L., Seale, L.D., Florea, L.J., Brinkmann, R., 2008. Using ALSM to map
648     sinkholes in the urbanized covered karst of Pinellas County, Florida—2. Accuracy
649     statistics. Environ. Geol. 54, 1007–1015.

650 Wolanski, E., Mazda, Y., Ridd, P., 1993. Mangrove hydrodynamics. Trop. mangrove
651     Ecosyst. 43–62.

652

653

654 **Tables**

| Time Step | Start | End | Duration | Quadripoles | | |
|---|---|---|---|---|---|---|
| 1 | *12:18:39* | *13:05:49* | *0:47:10* | *1219* | | rising tide |
| 2 | **13:46:05** | **14:32:37** | **0:46:32** | **1146** | day 1 | |
| 3 | **18:45:29** | **19:31:38** | **0:46:09** | **1049** | | falling tide |
| 4 | 19:32:57 | 20:19:34 | 0:46:37 | 1047 | | |
| 5 | 20:29:51 | 21:16:41 | 0:46:50 | 1048 | | |
| 6 | **21:20:37** | **22:08:00** | **0:47:23** | **1048** | night | |
| 7 | **0:01:16** | **0:47:28** | **0:46:12** | **1048** | | rising tide |
| 8 | **3:09:18** | **3:57:04** | **0:47:46** | **1049** | | |
| 9 | 4:40:01 | 5:26:26 | 0:46:25 | 1048 | | |
| 10 | 6:38:22 | 7:26:26 | 0:48:04 | 1049 | | falling tide |
| 11 | **7:44:00** | **8:30:43** | **0:46:43** | **1045** | day 2 | |
| 12 | **8:34:44** | **9:22:03** | **0:47:19** | **1049** | | |
| 13 | **10:45:12** | **11:34:33** | **0:49:21** | **1045** | | |

*Table 1 Data acquisition schedule. Only time steps that shown significant change*
*(**bold**) from the initial time step (italics) are presented in this paper.*

655
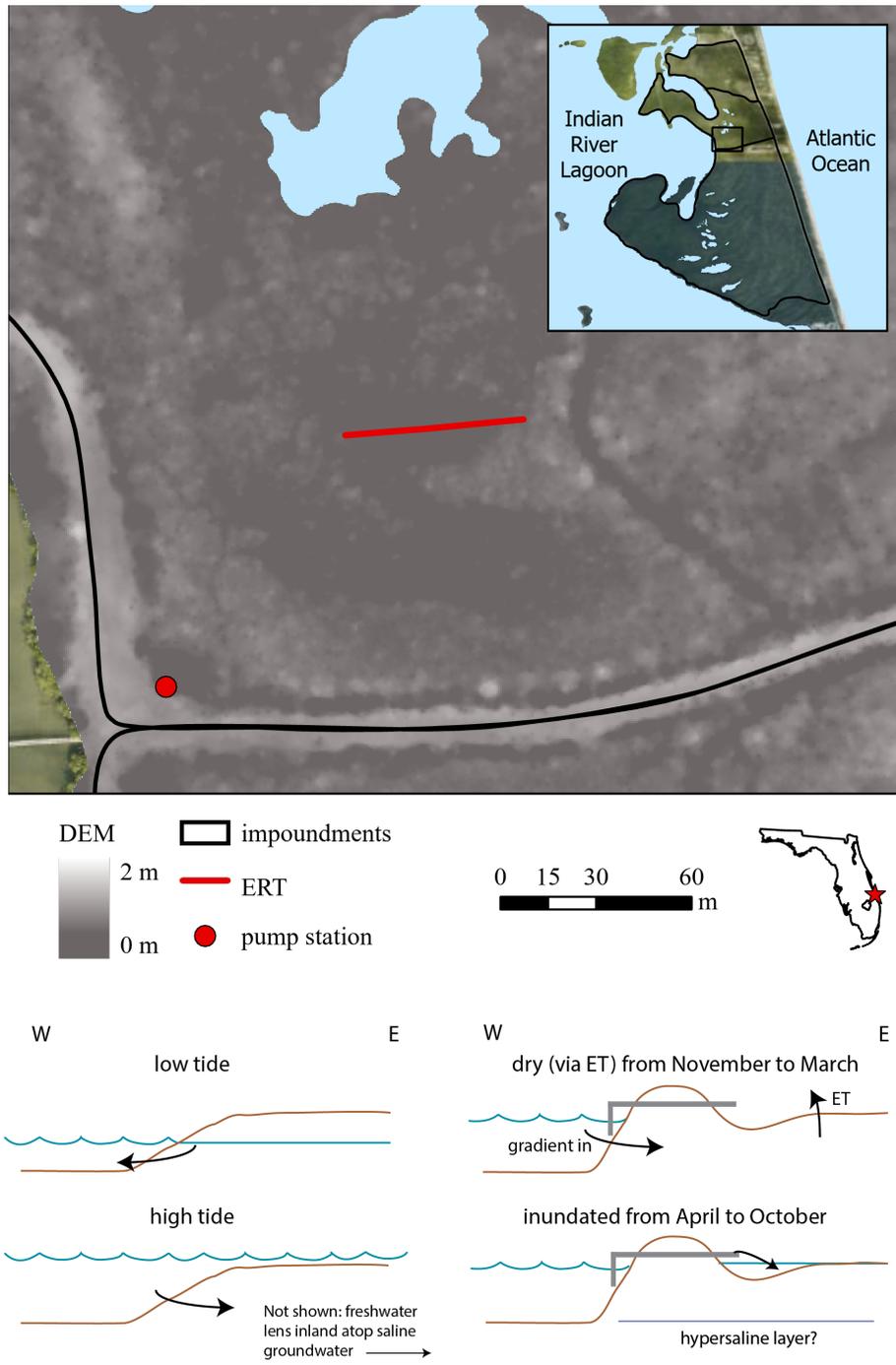
*Figure 1 Top: Digital elevation map of Imp-24: a mosquito-control impoundment on the west side on North Hutchinson Island, Florida, USA. Bottom: Cross-sectional schematic of free flowing system verses an impounded system at the study site including the current inundation schedule. The impoundment is an earthen dike that prevents surface water exchange between impoundments to the north and south and the brackish, tidal lagoon to the west. Impoundment water levels are measured at the pump station (not shown), which is in a trench between the dike and mangrove forest.*
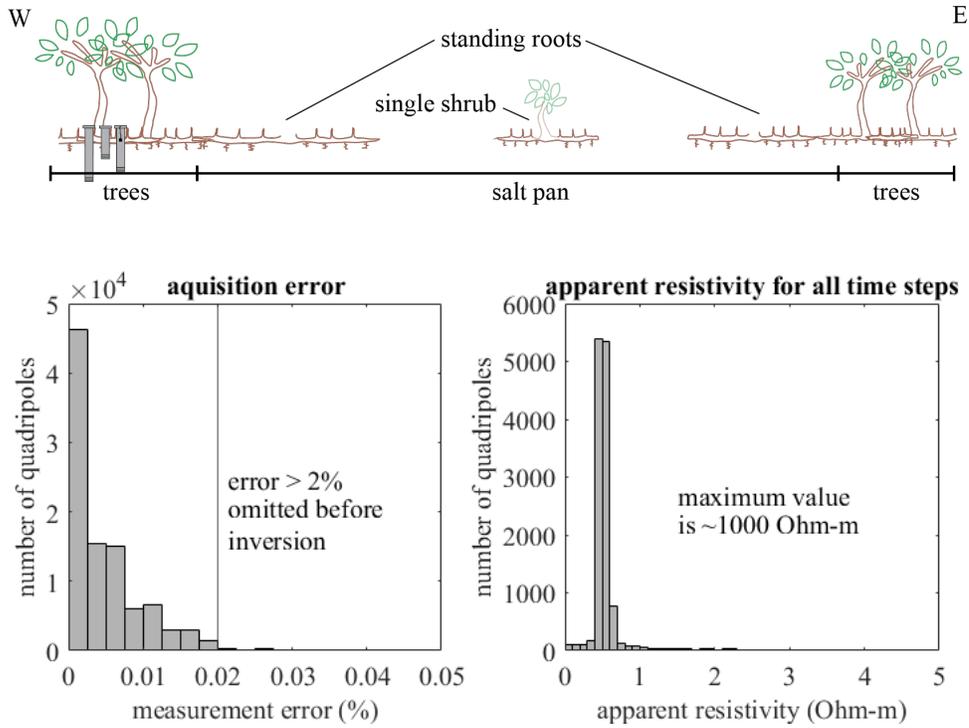
*Figure 2 Top: ERI transect crosses through small-stature mangrove trees and a salt flat with a single mangrove shrub. Bottom: Histograms of ER instrument acquisition error and apparent resistivity from all timesteps.*
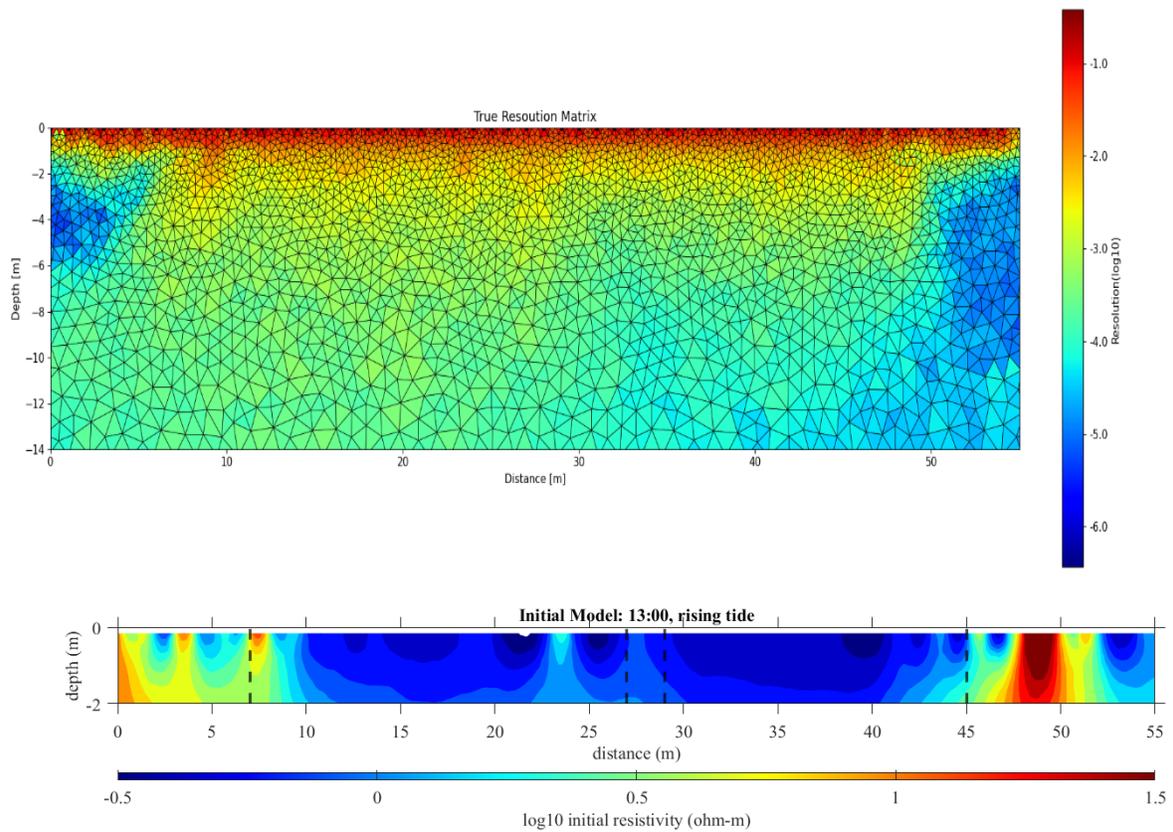
Figure 3 Top: True resolution matrix calcuated for the first time step. The best resolution is in the first two meters of the subsurface. The very low resolution at the edges (blue) are areas without data coverage. Bottom: 22°C equivalent resistivity of the first two meters from the first time step (day 1, 13:00.) Black dashed lines delineate the boundary between tree groupings and the salt flat with scattered standing roots. The salt flat is an order of magnitude less resistive than the vegetated zones on either side. The whole profile exhibits very low resistivity values indicative of the hypersaline and wet environment.
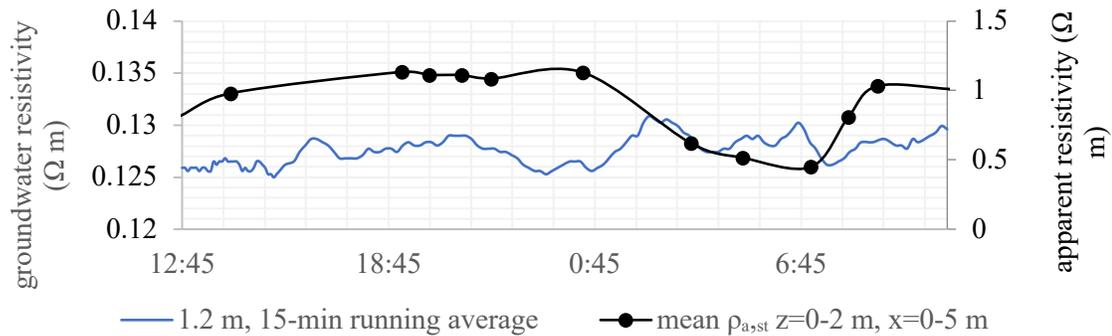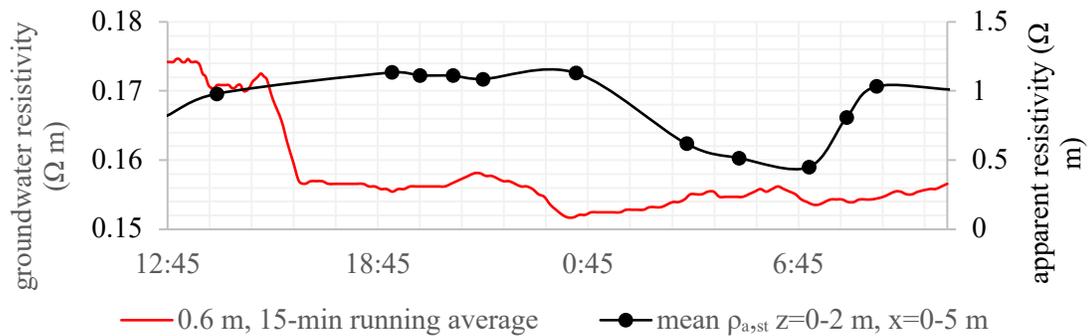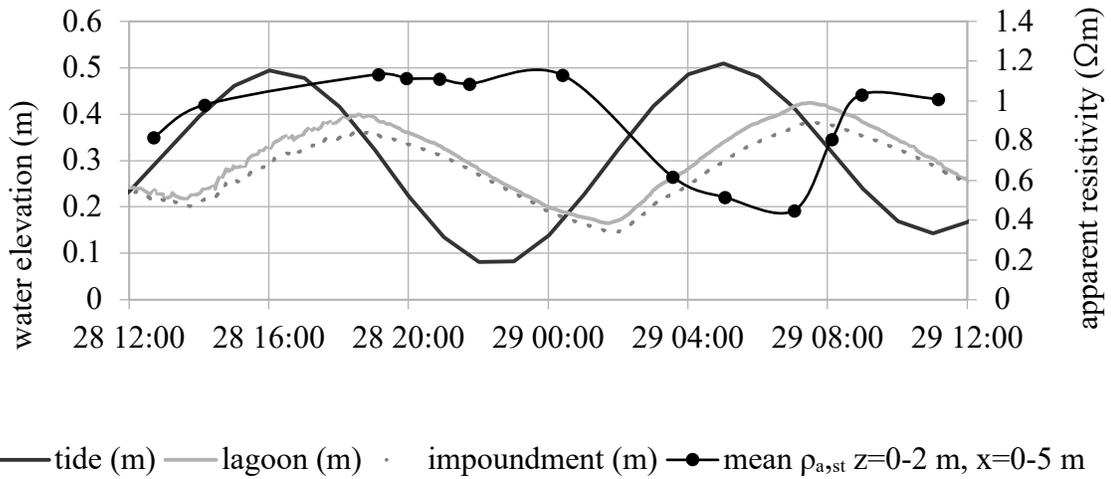
660

*Figure 4 Water measurements during the resistivity survey and raw ERI measurements. The 22°C equivalent mean apparent resistivity ($\rho_{a,st}$) from the top 2 meters for each time step plotted with tidal cycle (top) recorded in the lagoon, the trench between the earthen dike and mangrove forest, and an inlet to the south. The 22°C equivalent mean apparent resistivity ($\rho_{a,st}$) for each time step (from the top 2 meters and first 5 meter along the transect) plotted with a 15-min running average of groundwater resistivity at 0.6 m depth (middle) and 1.2 m depth (bottom).*

661

662
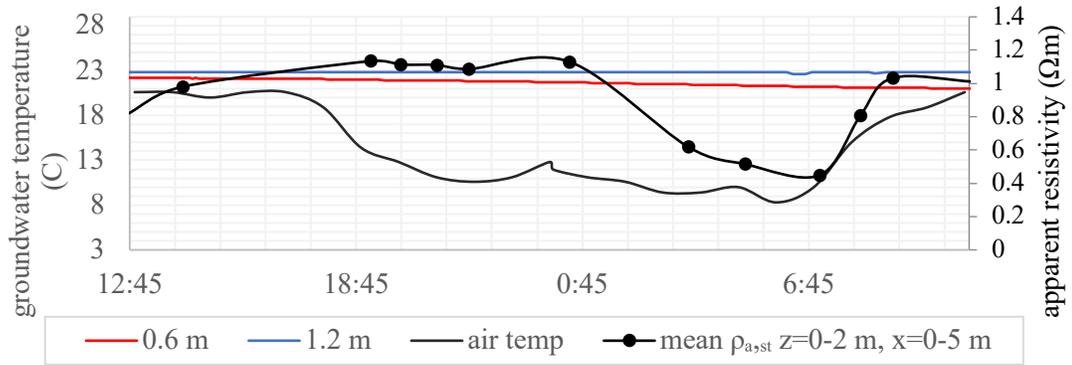


*Figure 5 Air temperature plotted with groundwater temperature at 0.6 and 1.2 meters depth and the 22°C equivalent mean apparent resistivity ($\rho_{a,st}$) from the top 2 meters of each time step.*

663

15:00, rising tide

19:00, sunset falling tide

22:00, falling tide 1

00:30, rising tide

03:30, rising tide

07:00, sunrise falling tide 2

08:00, falling tide

11:00, falling tide

Depth (m)

1  2  3  4  5  6  7  8  9  10
20.2°C equivalent resistivity (Ωm)

-2  -1.5  -1  -0.5  0  0.5  1  1.5  2
difference in resistivity from initial model (Ωm)
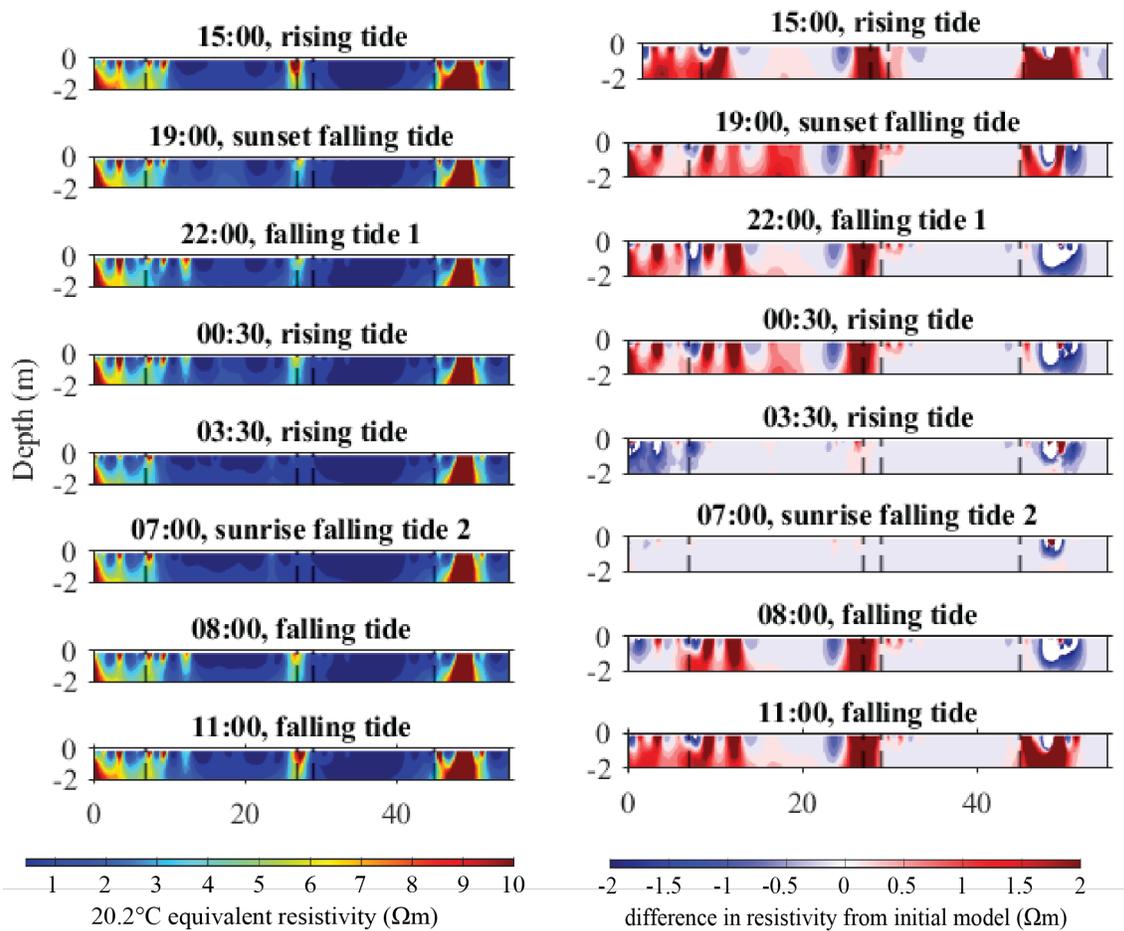
664

*Figure 6 Selected profiles from the time lapse survey. Profiles on the left display 22°C equivalent resistivity ($\rho_{st}$) for a given time step. Profiles on the right display the resistivity difference from the initial model collected at approximately 13:00 on day 1 (rising tide). Black dashed line delineate vegetation zones: dense scrub mangrove trees cover the east and west end of the transect (0-7 m and 45-55 m, respectively); a salt flat with some standing roots define much of the center of the profile. A single scrub tree is in the middle of the salt flat at approximately 29 m.*

31
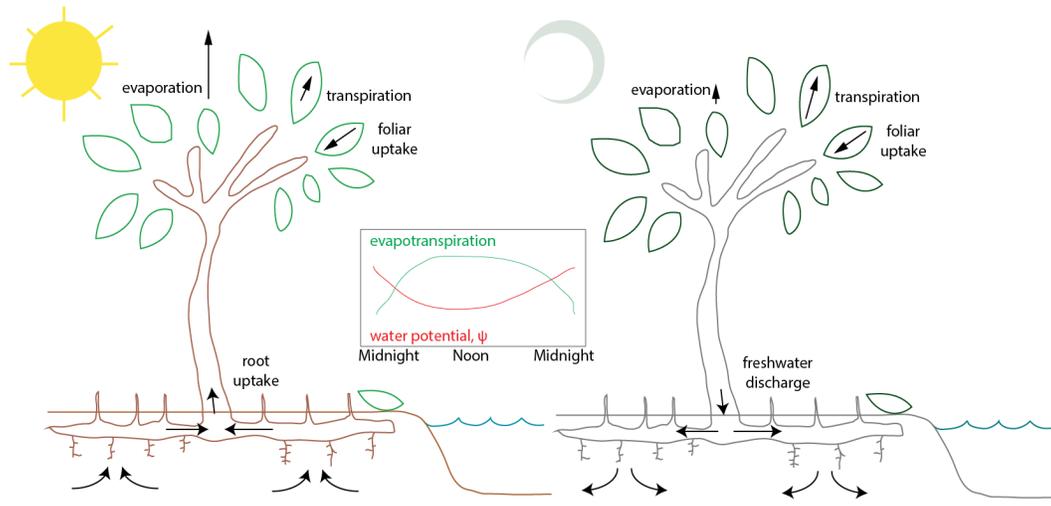
Figure 7 Suggested diel salt cycle for a black mangrove as suggested by time-lapse ERI results. The cycle contains a period of water uptake that slows down at sunset. Water pressure potential in the roots increases enough for water and salts to flow back into the soil (hydraulic redistribution.) Hydraulic redistribution starts before midnight and continues until sunrise. Transpiration and foliar uptake rates will depend on Original image from Alongi and Brinkman (2011).